CHAPTER 30

Time-Dependent Mild Slope Equation for Random Waves

Yasuhiro Kubo[1] Yasuo Kotake[2], Masahiko Isobe[2]
and Akira Watanabe[2]

A time-dependent mild slope equation is derived to simulate the deformation of irregular waves due to refraction, diffraction and breaking. It is based on Berkhoff's mild slope equation, but the resulting model is capable of simulating the time evolution of irregular wave profiles. The validity of the model is verified through comparisons with experimental data in a wave flume. Application examples for two-dimensional problems are given.

1 Introduction

The mild slope equation derived by Berkhoff (1972) has widely been used in the numerical calculation of refraction and diffraction of regular waves. However, it is well known that the randomness of sea waves has a significant effect on the wave height distribution due to refraction and diffraction.

In this paper a governing equation for calculating the time evolution of random waves due to refraction and diffraction is derived on the basis of the mild slope equation. An energy dissipation term is added to model the wave breaking. To examine the validity of the equation, the results of calculation are compared with measurements in a wave flume. Examples of model application to two-dimensional random wave computation are also given.

[1]Tokyo Electric Power Co. Ltd.
[2]Dept. of Civil Eng. , Univ. of Tokyo ,Bunkyo–ku , Tokyo , 113 , Japan

2 Derivation of Governing Equation

The mild slope equation derived by Berkhoff (1972) is written as

$$\nabla(cc_g\nabla\widehat{\eta}) + k^2cc_g\widehat{\eta} = 0 \tag{1}$$

where c is the wave celerity, c_g the group velocity, k the wave number, and ∇ the horizontal gradient operator. The quantity $\widehat{\eta}$ denotes the complex amplitude of the water surface elevation, by which the water surface elevation η is expressed as $\eta = \mathrm{Re}[\widehat{\eta}e^{-i\omega t}]$ (ω: the angular frequency). In the above equation, the quantities cc_g and k^2cc_g depend on the frequency, which restricts the applicability of the mild slope equation to waves with a single frequency.

For random waves, the water surface elevation is expressed as the superposition of component waves :

$$\eta = \mathrm{Re}[\sum_{m=1}^{\infty} \widehat{\eta}_m e^{-i\omega_m t}] \tag{2}$$

where ω_m is the angular frequency and $\widehat{\eta}_m$ the complex amplitude of the m-th component waves.

To apply the mild slope equation to the analysis of random wave transformation, we define a variable $\tilde{\eta}$ such that

$$\eta = \mathrm{Re}[\tilde{\eta}e^{-i\bar{\omega}t}] \tag{3}$$

where $\bar{\omega}$ is a representative angular frequency such as the peak frequency. Comparing this with Eq. (2), we have

$$\eta = \mathrm{Re}[\sum_{m=1}^{\infty} \tilde{\eta}_m e^{-i\bar{\omega}t}] \tag{4}$$

and

$$\tilde{\eta}_m = \widehat{\eta}_m e^{-i\Delta\omega_m t} \tag{5}$$

where $\Delta\omega_m = \omega_m - \bar{\omega}$. The variable $\tilde{\eta}_m$ is a function of time t, for which

$$\frac{\partial\tilde{\eta}_m}{\partial t} = -i\Delta\omega_m\tilde{\eta}_m \tag{6}$$

The quantity $\tilde{\eta}_m$ is a function of time t, it is a solution of Eq. (1) as well as $\widehat{\eta}_m$. Therefore, we can rewrite Eq. (1) as

$$\nabla[(cc_g)_m\nabla\tilde{\eta}_m] + (k^2cc_g)_m\tilde{\eta}_m = 0 \tag{7}$$

Since the quantities $(cc_g)_m$ and $(k^2cc_g)_m$ depend on the angular frequency ω_m, it is not possible to superimpose Eq. (7) for all component waves and calculate $\tilde{\eta}$

directly. Therefore, we modify Eq. (7) and change the quantities cc_g and k^2cc_g into constants independent of component angular frequencies.

If we expand the quantities $(cc_g)_m$ and $(k^2cc_g)_m$ into Taylor series of $\Delta\omega_m$ and eliminate powers of $\Delta\omega_m$ using relations such as $-i\Delta\omega_m\tilde{\eta}_m = \partial\tilde{\eta}_m/\partial t$ and $(-i\Delta\omega_m)^2\tilde{\eta}_m = \partial^2\tilde{\eta}_m/\partial^2 t$, we can obtain an equation in which all the quantities can be determined from the representative frequency only.

For example, by truncating the Taylor series at the first order, the first and second terms in Eq. (7) are expressed as

$$(cc_g)_m\nabla\tilde{\eta}_m = [\overline{cc_g} + \overline{\frac{d(cc_g)}{d\omega}}\Delta\omega_m]\nabla\tilde{\eta}_m = \overline{cc_g}\nabla\tilde{\eta}_m + i\overline{\frac{d(cc_g)}{d\omega}}\nabla\left(\frac{\partial\tilde{\eta}_m}{\partial t}\right) \tag{8}$$

$$(k^2cc_g)_m\tilde{\eta}_m = [\overline{k^2cc_g} + \overline{\frac{d(k^2cc_g)}{d\omega}}\Delta\omega_m]\tilde{\eta}_m = \overline{k^2cc_g}\tilde{\eta}_m + i\overline{\frac{d(cc_g)}{d\omega}}\frac{\partial\tilde{\eta}_m}{\partial t} \tag{9}$$

where all the quantities $\overline{cc_g}$, $\overline{d(cc_g)/d\omega}$, $\overline{k^2cc_g}$ and $\overline{d(k^2cc_g)/d\omega}$ are constants. Substitution of Equations (8) and (9) into Eq. (7) yields

$$\nabla(\bar{\alpha}\nabla\tilde{\eta}_m) + i\nabla[\bar{\beta}\nabla(\frac{\partial\tilde{\eta}_m}{\partial t})] + \bar{k}^2\bar{\alpha}\tilde{\eta}_m + i\bar{\gamma}\frac{\partial\tilde{\eta}_m}{\partial t} = 0 \tag{10}$$

$$\bar{\alpha} = \bar{c}\bar{c}_g \tag{11}$$

$$\bar{\beta} = \frac{\bar{c}}{\bar{k}}[-2(1-\bar{n}) + \frac{1}{2\bar{n}}(2\bar{n}-1)\{1-(2\bar{n}-1)\cosh 2\bar{k}d\}] \tag{12}$$

$$\bar{\gamma} = \bar{k}\bar{c}[2\bar{n} + \frac{1}{2\bar{n}}(2\bar{n}-1)\{1-(2\bar{n}-1)\cosh 2\bar{k}d\}] \tag{13}$$

$$\bar{n} = 1/2(1 + 2\bar{k}d/\sinh 2\bar{k}d) \tag{14}$$

Then, superposition of Eq. (10) for an infinite number of component waves yields

$$\nabla(\bar{\alpha}\nabla\tilde{\eta}) + i\nabla[\bar{\beta}\nabla(\frac{\partial\tilde{\eta}}{\partial t})] + \bar{k}^2\bar{\alpha}\tilde{\eta} + i\bar{\gamma}\frac{\partial\tilde{\eta}}{\partial t} = 0 \tag{15}$$

which is termed as a time-dependent mild slope equation for random waves. For random incident waves, $\tilde{\eta}$ along the boundary is determined by Eq. (4), and then $\tilde{\eta}$ in the calculation domain can directly be calculated by Eq. (15).

The above expansion of the quantities cc_g and k^2cc_g into the first-order Taylor series of $\Delta\omega_m$ is equivalent to approximating them as linear functions of ω. Fig. 1 illustrates the accuracy of the approximation. As seen in Fig. 1, the error is insignificant when the deviation of the frequency from the representative value is small.

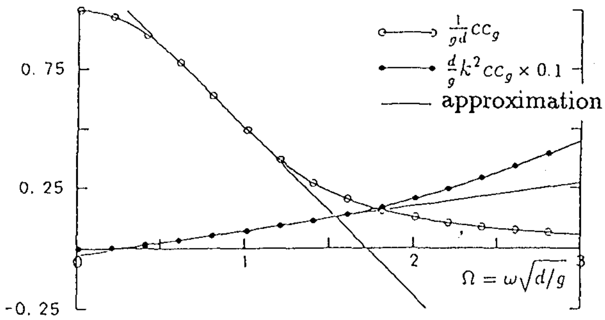

Fig. 1: Accuracy of the approximated quantities

3 Modeling of Wave Breaking

To incorporate energy dissipation due to wave breaking, an empirical energy dissipation term based on the model presented by Isobe(1986) is added to Eq. (15):

$$\nabla(\bar{\alpha}\nabla\tilde{\eta}) + i\nabla[\bar{\beta}\nabla(\frac{\partial\tilde{\eta}}{\partial t})] + \bar{k}^2\bar{\alpha}(1+if_D)\tilde{\eta} + i\bar{\gamma}(1+if_D)\frac{\partial\tilde{\eta}}{\partial t} = 0 \qquad (16)$$

where f_D is the energy dissipation coefficient.

It is convenient to evaluate f_D by using spatial wave profiles because time series of the spatial profile are obtained as a solution of Eq. (16). In the procedure, we first divide the spatial wave profiles into individual waves by the zero-up crossing method from offshore to onshore as shown in Fig. 2.

To judge the breaking of individual waves, the amplitude to water depth ratio,

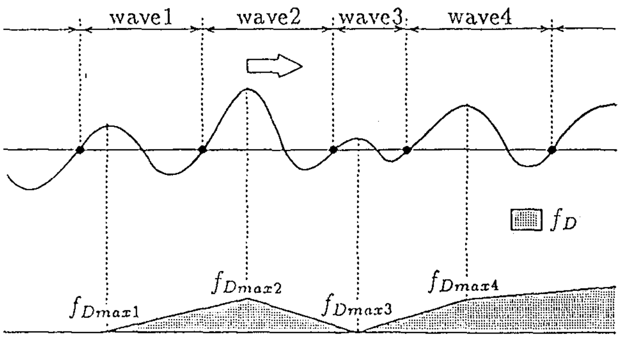

Fig. 2: Evaluation of energy dissipation function due to wave breaking

γ, is introduced as follows:

$$\gamma = |\tilde{\eta}|/d \tag{17}$$

where $|\tilde{\eta}|$ is the amplitude at the wave crest and d the water depth. If γ is greater than γ_b which is a critical value of wave breaking and determined by Eq. (18), the individual wave is judged to be breaking.

$$\gamma_b = 0.8\gamma_b' \tag{18}$$

$$\gamma_b' = 0.53 - 0.3\exp(-3\sqrt{d/L_0}) + 5\tan^{\frac{3}{2}}\beta\exp\{-45(\sqrt{d/L_0} - 0.1)^2\} \tag{19}$$

where L_0 is the representative wavelength in deep water and $\tan\beta$ the bottom slope. The value 0.8 in Eq. (18) is introduced to consider that random waves are easier to break than regular waves. After breaking, if γ becomes smaller than γ_r which is a critical value of wave recovery determined by Eq. (20), the individual wave is judged to have recovered.

$$\gamma_r = 0.135 \tag{20}$$

To evaluate the spatial distribution of the energy dissipation coefficient, we first determine $f_{D\mathrm{max}}$ at each crest of breaking waves by Eq. (21), then obtain the energy dissipation coefficient f_D by interpolating $f_{D\mathrm{max}}$ linearly as shown in Fig. 2, and finally calculate the water surface profile at the next time step.

$$f_{D\mathrm{max}} = \frac{5}{2}\tan\beta\sqrt{\frac{1}{k_0 d}}\sqrt{\frac{\gamma - \gamma_r}{\gamma_s - \gamma_r}} \tag{21}$$

$$\gamma_s = 0.4 \times (0.57 + 5.3\tan\beta) \tag{22}$$

where k_0 is the representative wave number. The same procedure is repeated for arbitrary time steps.

4 Boundary conditions

The open boundary condition, which allows outgoing waves to propagate freely, is not easy to implement. In addition, along the offshore boundary, the incident waves should be introduced.

We apply a method presented by Ohyama *et al.*(1990) to the open boundaries. In the method, the energy of outgoing waves is absorbed in the energy dissipation layer which is added outside of the boundary. To introduce the incident waves from the offshore boundary, terms due to an exciting force are added on the right hand side:

$$\begin{aligned}\nabla(\bar{\alpha}\nabla\tilde{\eta}) + i\nabla[\bar{\beta}\nabla(\frac{\partial\tilde{\eta}}{\partial t})] + \bar{k}^2\bar{\alpha}(1 + if_D)\tilde{\eta} + i\bar{\gamma}(1 + if_D)\frac{\partial\tilde{\eta}}{\partial t} \\ = \nabla(\bar{\alpha}\nabla\tilde{\eta}_{\mathrm{in}}) + i\nabla[\bar{\beta}\nabla(\frac{\partial\tilde{\eta}_{\mathrm{in}}}{\partial t})] + \bar{k}^2\bar{\alpha}(1 + if_D)\tilde{\eta}_{\mathrm{in}} + i\bar{\gamma}(1 + if_D)\frac{\partial\tilde{\eta}_{\mathrm{in}}}{\partial t}\end{aligned} \tag{23}$$

where $\tilde{\eta}_{\rm in}$ is the complex amplitude due to the incident waves. The above equation is obtained by substituting component, $\tilde{\eta}_{\rm out} = \tilde{\eta} - \tilde{\eta}_{\rm in}$, due to outgoing waves for $\tilde{\eta}$ in Eq. (16).

5 Application and Results

Time-evolutional solutions can be obtained from Eq. (16) by using a finite difference method.

Numerical calculations for the present equation are carried out for one-dimensional cases by using Crank-Nicholson method. Figures 3 and 4 show the result for two component waves with slightly different frequencies, $0.9\bar{\omega}$ and $1.1\bar{\omega}$ ($\overline{\omega}$: the mean angular frequency). Fig. 3 is for deep water and Fig. 4 for shallow water. Spacial wave profiles are shown at four time steps from the top to the

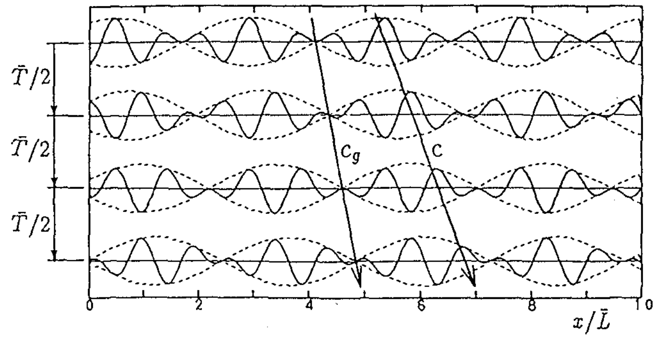

Fig. 3: Propagation of two-component waves (deep water)

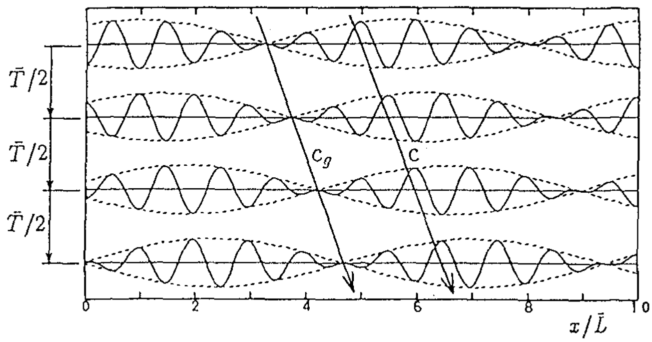

Fig. 4: Propagation of two-component waves (shallow water)

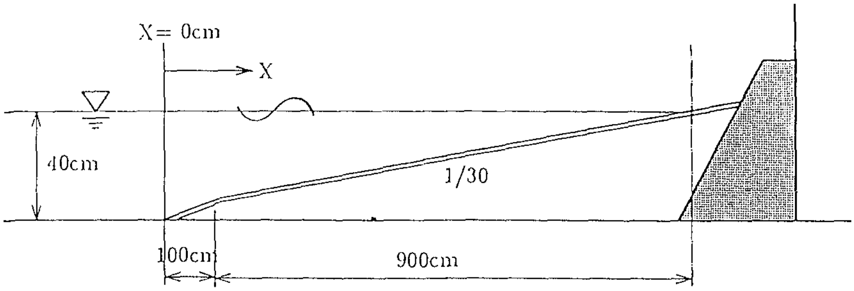

Fig. 5: Wave flume and bottom configuration

bottom with an interval of a half of the mean period. It seems in Fig. 3 that waves propagate with the wave celerity c, while wave groups propagate with the group velocity c_g. This can not be reproduced by the previous time-dependent mild slope equation.

Results of numerical calculations are compared with experiments for the wave transformations on a slope to confirm the validity of the present equation. The data were obtained by Watanabe *et al.*(1988) in a wave flume shown in Fig. 5. Figures 6 and 7 compare the measured and calculated wave height variations of random waves on a beach with a slope of 1/30 . The offshore boundary condition is given at $x = -40$cm and the shoreline is located at $x = 1000$cm. Fig. 6 is for the plunging-breaker (case 1), while Fig. 7 for the spilling-breaker (case 2).

The peak frequency f_p and the significant wave height $H_{1/3}$ of the incident waves are 0.5Hz and 5.4cm for case 1, and 0.75Hz and 9.2cm for case 2. In the numerical calculations, the incident waves are given by synthesizing component waves with frequency $0.25f_p \sim 2.5f_p$, which were extracted from the measured water surface elevation at the offshore boundary by using FFT. The grid size Δx is 10cm and the time interval Δt is 0.02s.

In Fig. 6, the calculated significant wave height variations does not agree well with the measured one near the breaking point since the present equation is linear. However, the root mean square of the water surface variation is predicted well due to the empirical formulation of the dissipation term.

Fig. 8 compares the measured and calculated water surface fluctuations for the case 2. Fig. 8 (a) is for the offshore boundary, Fig. 8 (b) for the offshore zone, Fig. 8 (c) for the average breaking point and Fig. 8 (d) for the surf zone. As seen in Fig. 8 (b), a good agreement is obtained in the offshore zone, but in Fig. 8 (d) the difference is large. Owing to the linearity of the equation, the

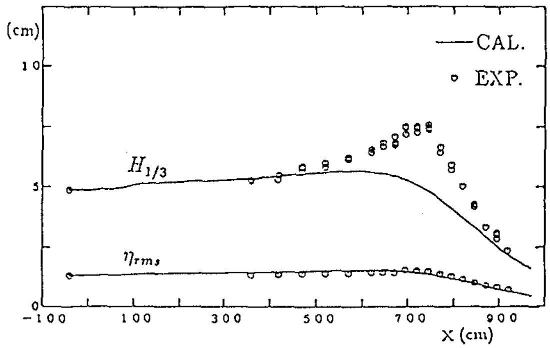

Fig. 6: Comparison of the measured and calculated wave height variations (case 1:$H_{1/3}$ = 5.4cm, f_p = 0.5Hz)

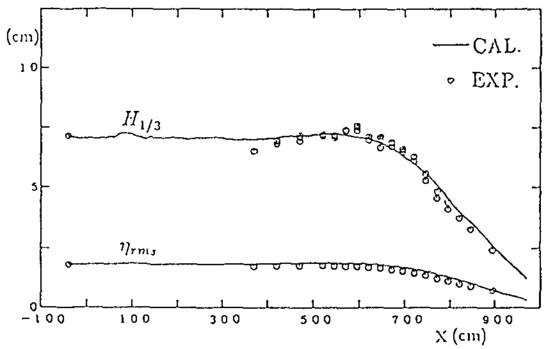

Fig. 7: Comparison of the measured and calculated wave height variations (case 2:$H_{1/3}$ = 9.2cm, f_p = 0.75Hz)

present equation can not reproduce the non-linear properties such as skewness of the wave profile. However, the transformation of wave groups is well reproduced.

As examples of application to two-dimensional problems, wave fields on a uniform slope and around a detached breakwater are calculated by the present equation. For two-dimensional problems, the ADI method is used because it reduces the memory size and computation time.

Fig. 9 shows the calculation domain. The contour lines are shown for the energy dissipation coefficient f_D in the energy dissipation layer. The layer is taken thicker along the offshore boundary than along the onshore boundary because of the difference in wavelengths. The grid size Δl is 2m and the time interval Δt is 0.02s.

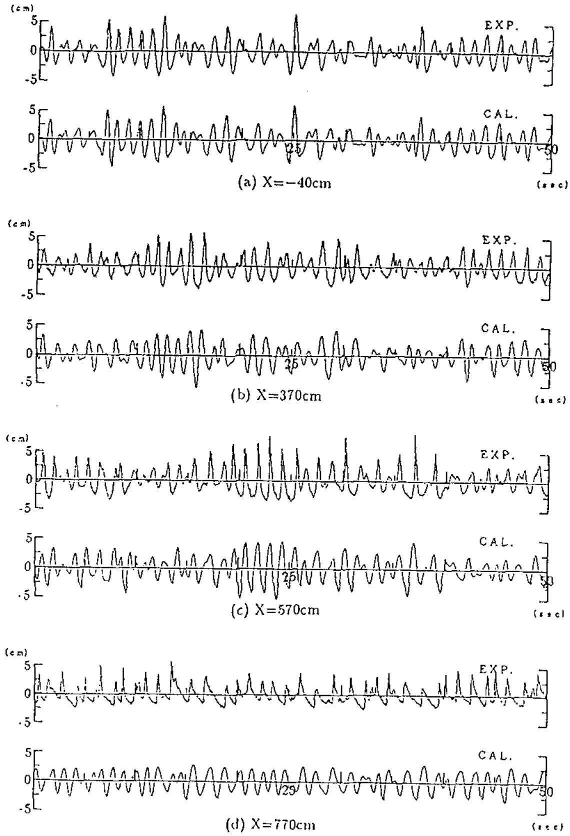

Fig. 8: Comparison of the measured and calculated wave surface fluctuations (case2)

Numerical calculations are carried out for two cases: for regular waves and multidirectional irregular waves. The wave period or significant wave period is 6s, and the wave height or significant wave height is 1m in deep water.

The frequency spectrum of the incident irregular waves is of the Bretshneider-

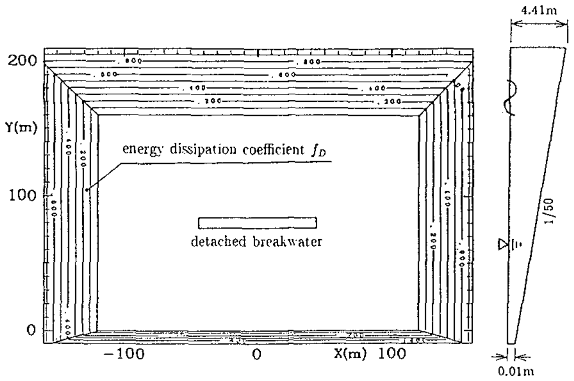

Fig. 9: Calculation domain

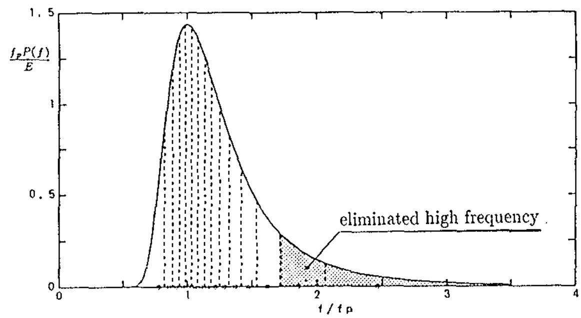

Fig. 10: The frequency spectrum of incident waves

Mitsuyasu spectrum and the Mitsuyasu-type directional distribution function is used with $S_{\max} = 10$. The incident irregular waves are given by the double summation method in which 13 frequency components and 15 directional components are used. High frequency components are cut as shown in Fig. 10, because the applicability range of the present equation is restricted within a narrow band.

Figures 11 (a) and 11 (b) compare the analytical and numerical solution of wave height variations of component waves due to refraction. Fig. 11 (a) is for the longest wave period 8.09 s and Fig. 11 (b) for the shortest wave period 3.89s. In these figures, the calculated solutions agree well with the analytical ones.

Figures 12 (a) and 12 (b) show the results of the numerical calculation of the wave field around a detached breakwater for regular and irregular waves, respectively. Figures 13 and 14 show the wave height variations along the X- and Y-axis. As seen in these figures, the distribution of wave height is smoother

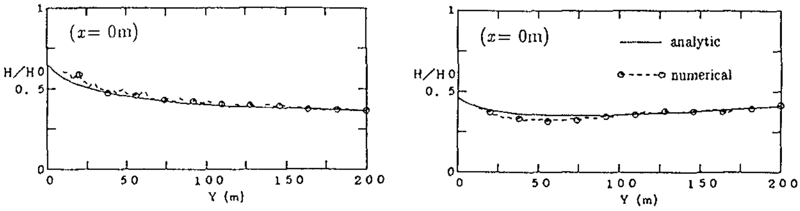

(a) the longest wave period 8.09s (b) the shortest wave period 3.89s

Fig. 11: Comparison of the analytical and calculated wave height variations of component wave

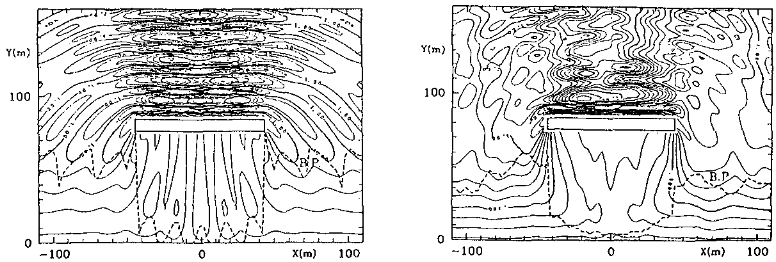

(a) regular wave field (b) irregular wave field

Fig. 12: Comparison of the regular wave field and irregular wave field around a detached breakwater

for the irregular waves because of the frequency and directional distribution. For the regular waves, nodes and anti-nodes are clearly seen. The asymmetrical distribution of wave height for irregular waves is due to a statistical variation because the significant wave height is obtained by using $H_{1/3} = 4.004\eta_{\mathrm{rms}}$, where η_{rms} is the root mean square of the water surface elevation.

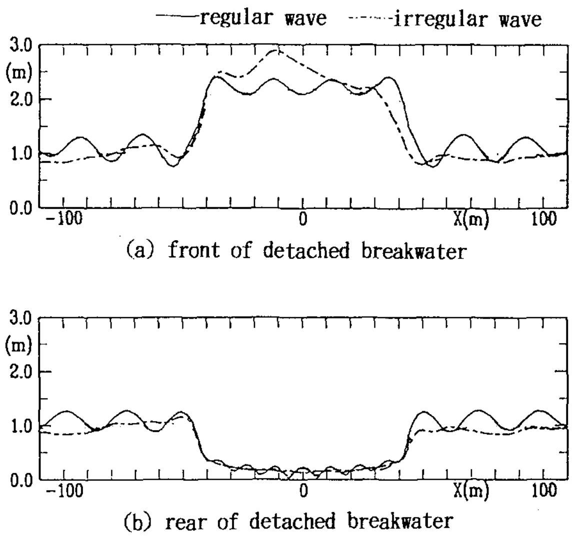

Fig. 13: Comparison of wave height variations of regular and irregular waves along the x-axis

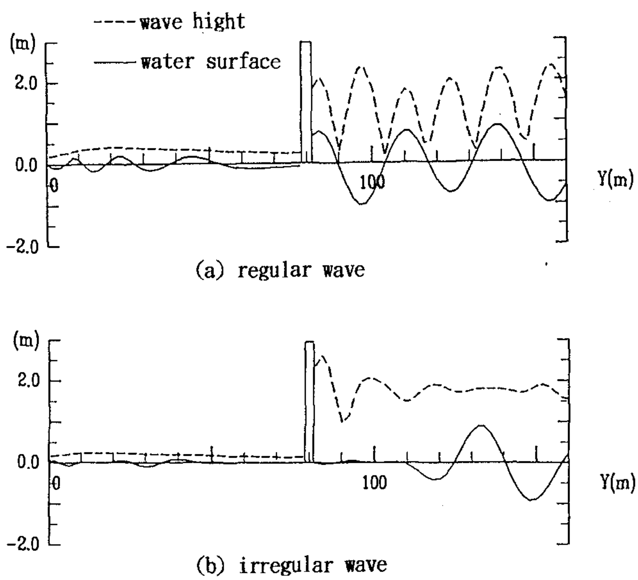

Fig. 14: Comparison of wave height variations of regular and irregular waves along the y-axis.

6 Conclusion

A time-dependent mild slope equation for random waves was derived from Berkhoff's mild slope equation. An advantage of the present equation is that it allows to calculate the time evolution of the random wave transformation due to refraction and diffraction and can easily incorporate a breaking wave model. The results of numerical calculations were compared with theoretical predictions and laboratory data, which confirmed the validity of the present equation.

References

Berkhoff, J. C. W.(1972) : Computation of combined refraction-diffraction, Proc. 13th Int. Conf. on Coastal Eng., pp. 191-203.

Isobe, M.(1987) : A parabolic equation model for transformation of irregular waves due to refraction, diffraction and breaking, Coastal Eng. in Japan, Vol. 30, No. 1, pp. 38-48.

Ohyama, T. and N. Nadaoka (1990) : Modeling the transformation of nonlinear waves passing over a submerged step, Proc. Japanese Conf. on Coastal Eng., JSCE, Vol. 37, pp. 16-20 (in Japanese).

Watanabe, A. , M. Isobe , T. Izumiya and H. Nakano (1988) : Analysis for shoaling and breaking of random waves with time-dependent mild-slope equations, Proc. 35th Japanese Conf. on Coastal Eng., pp. 173-177 (in Japanese).